https://doi.org/10.5194/egusphere-2026-188
Preprint. Discussion started: 29 January 2026

Technical note: tidal motions in the deep Mediterranean

by Hans van Haren

Royal Netherlands Institute for Sea Research (NIOZ), P.O. Box 59, 1790 AB Den Burg, the Netherlands.
e-mail: hans.van.haren@nioz.nl

https://doi.org/10.5194/egusphere-2026-188
Preprint. Discussion started: 29 January 2026

Abstract. The Mediterranean Sea is known for its limited tidal motions. For example, surface barotropic tidal elevations have an amplitude of 0.1 m in the Northwestern Mediterranean. Nevertheless, these small tides are noticeable in temperature records at the 2500-m deep seafloor, but only under near-homogeneous conditions when buoyancy frequency N < f, the inertial frequency. After transfer of pressure to temperature units via the local adiabatic lapse rate, the observed internal-wave temperature signals may thus be corrected for 1.5×10^{-5}-°C amplitude semidiurnal barotropic tides. The remaining baroclinic tides are embedded in the broad and featureless inertio-gravity wave band, with some energy enhancement near its boundaries, also under tenfold-larger energetic stratified water conditions.

1 Introduction

In the over 2000-m deep Western Mediterranean Sea milli- to centi-degree variations in temperature characterize all dynamical processes. This deep sea may be void of sunlight and its waterflow may be relatively slow at speeds of 0.05 m s^{-1}, it is not stagnant but requires precise instrumentation for studying such processes. Above the generally flat seafloor in the vicinity of its northern continental shelf, dynamical processes include a large-scale boundary flow (e.g., Crepon et al., 1982), with meanders and eddies varying at 1-10 day and 1-10 km sub-mesoscales, as well as at 10-30 day and 10-100 km mesoscales. The variations result from instabilities of the boundary flow and associated fronts, horizontal density variations between coastal and offshore water masses. These are strongest near the surface, but can be traced all the way to the seafloor in weaker form. Shorter-period variations involve waves in the interior of the sea, notably at near-inertial scales, as transients following passages of atmospheric disturbances induced by, e.g., varying winds from the nearby mountain ranges like the Alps. Near-inertial motions can penetrate as 'internal waves' into the deep sea, e.g. via trapping by (sub-)mesoscale eddies (Kunze, 1985). They may set-up shorter scale internal waves that eventually dissipate their energy through irreversible turbulence when they break.

In contrast with most seas and oceans, tides are generally weak in the Mediterranean, with a few local exceptions. Although the weak tides reduce the amount of internal-wave energy by about 60% (Wunsch and Ferrari, 2004), internal-wave breaking constitutes a non-negligible generator of turbulence besides geothermal heating in the deep Mediterranean (e.g., van Haren et al., 2014; Ferron et al., 2017;

https://doi.org/10.5194/egusphere-2026-188
Preprint. Discussion started: 29 January 2026

van Haren et al., 2026). The existing motions make the Mediterranean Sea a sample for ocean-dynamics processes (Garrett, 1994).

The weak tides in most of the Mediterranean result from poor resonance conditions so that they reflect direct generation by the Moon-Sun system. In the Northwestern Mediterranean typical sea-level amplitudes are 0.1 m (https://www.tide-forecast.com/locations/Toulon-France/tides/latest). These 'barotropic' surface tides, which have unattenuated amplitude from surface to bottom, may generate internal 'baroclinic' tides, which have distinct amplitude and phase variations over short distances, when vertical density-stratification conditions are favourable.

In the deep Mediterranean however, the local mean buoyancy frequency has values of $N = O(f)$, $f = 2\Omega\sin\varphi$ denotes the inertial frequency or vertical Coriolis parameter at latitude φ and Ω the Earth rotational frequency. Under such weakly stratified conditions (van Haren and Millot, 2003), the frequency (ω) range of freely propagating internal waves spreads well into the sub-inertial, $\omega < f$, sub-mesoscale range as not only gravity but also Earth's rotational momentum play a role as restoring force (LeBlond and Mysak, 1978): inertio-gravity waves 'IGW'.

This because the common internal-wave band $f < \omega < N$, for strong stratification with $N >> f$ (LeBlond and Mysak, 1978), becomes modified by the effect of traditionally neglected horizontal Coriolis parameter $f_h = 2\Omega\cos\varphi$ under weakly stratified conditions. For $N = O(f)$, minimum IGW-bound $\omega_{min} \leq f$ and maximum IGW-bound $\omega_{max} \geq 2\Omega$ or N, whatever is largest, are functions of N, φ, and the direction of wave propagation (LeBlond and Mysak, 1978; Gerkema et al., 2008),

$$\omega_{max}, \omega_{min} = (A \pm (A^2-B^2)^{1/2})^{1/2}/\sqrt{2}, \quad (1)$$

in which $A = N^2 + f^2 + f_s^2$, $B = 2fN$, and $f_s = f_h\sin\alpha$, α the angle to φ. For $f_s = 0$ or $N >> 2\Omega$, the traditional bounds [f, N] are retrieved from (1). One effect of f_h is turbulent-convection in slantwise direction in the vertical, meridional z,y-plane, so that apparently stable stratification observed in z-direction may actually reflect homogeneous or unstable conditions in the tilted plane of planetary vorticity, except at the north pole (e.g., Straneo et al., 2002; Sheremet, 2004). Another effect of f_h is that semidiurnal tidal frequencies are always included in IGW, albeit for meridional propagation direction only.

https://doi.org/10.5194/egusphere-2026-188
Preprint. Discussion started: 29 January 2026

Internal-wave bounds may also vary due to (sub-)mesoscale motions. Local time- and space-varying horizontal waterflow differences such as in meanders and eddies can generate relative vorticity ζ, with reported amplitudes of up to |ζ| = f/2 around mid-depth in the Western Mediterranean (Testor and Gascard, 2006). This addition to planetary vorticity f widens the 'effective' near-inertial band by about ±0.2f (Kunze, 1985).

In this note, the contribution of barotropic and baroclinic tides to the potentially widened IGW in the deep Mediterranean is investigated using observations made at a large three-dimensional mooring array for improved statistics. Pressure information is used to separate dynamically unimportant barotropic tides, which appear as O(0.00001°C) amplitudes, from temperature records.

2 Materials and Methods

Nearly half-a-cubic-hectometer of deep Mediterranean seawater was measured every 2 s using 2925 self-contained high-resolution NIOZ4 T-sensors, which can also record tilt and compass. Temperature-only sensors were taped at 2-m intervals to 45 vertical lines 125-m tall (van Haren et al., 2021). In addition, two tilt-temperature sensors were attached near top and bottom of each line, which was tensioned to 1.3 kN by a single buoy above. Three buoys, equally distributed over the mooring-array, held an acoustic single-point Nortek AquaDopp current meter 'CM' that recorded waterflow and pressure at a rate of once per 600 s. The lines were attached at 9.5-m horizontal intervals to a steel-cable grid that was tensioned inside a 70-m diameter steel-tube ring, which functioned as a 140-kN anchor. This 'large-ring mooring' was deployed at the <1° flat and 2458-m deep seafloor of 42° 49.50′N, 006° 11.78′E, 10 km south of the steep continental slope in the NW-Mediterranean Sea, in October 2020.

Probably due to a format error, the T-sensors switched off unintentionally after maximum 20-months of data-recording. Tilt-temperature sensors recorded only 5.5 months of data, which data are not considered here. As with previous NIOZ4 T-sensors (for details see van Haren, 2018), the T-sensors' individual clocks were synchronized to a single standard clock every 4 hours, so that all T-sensors were recording data within 0.02 s. About 25 T-sensors failed mechanically. During post-processing, some 20 extra T-sensors are not further considered due to general electronics (noise) problems. Data from these

https://doi.org/10.5194/egusphere-2026-188
Preprint. Discussion started: 29 January 2026

sensors are not considered in spectral analyses and linearly interpolated between data from neighbouring sensors in other analyses. One near-bottom T-sensor failed. Instrumental bias was removed via vertical smoothing and via low-pass filtering. In addition, because vertical temperature (density) gradients are so small in the deep Mediterranean, reference was made to periods of typically one hour duration that were homogeneous with temperature variation smaller than instrumental noise level (van Haren, 2022).

For reference, a single shipborne Conductivity-Temperature-Depth 'CTD' profile was obtained within 1 km from the site of large-ring mooring, during the deployment cruise.

3 Results

The lower 500 m of the CTD-profile shows weak but stratified water 'SW' conditions down to $h \approx 300$ m from the seafloor, and near-homogeneous 'NH' conditions closer to the seafloor (Fig. 1a, b). The transition between the two conditions is quite abruptly in vertical density stratification. However, in both cases stratification is rather weak, with 100-m-scale buoyancy frequency $N \approx 2f$ under SW and $N < 0.5f$ under NH. The generally weak stratification implies that the adiabatic lapse rate Γ of compressibility dominates the variation in temperature with depth, especially for $h < 300$ m (Fig. 1a). Γ is a function of local salinity, temperature and pressure p, and amounts,

$$\Gamma = d\Theta/dp = 1.68\pm0.01\times10^{-8}\ ^{\circ}\text{C m}^2\ \text{N}^{-1}, \tag{2}$$

for the range in Fig. 1a.

The CTD-profile is representative for local conditions within the vertical range $h < 126$ m of moored instrumentation (cf. Fig. 1b) during about half their time underwater. During the remainder, SW conditions reach the moored instrumentation, either from above or from the side. They provide 124-m vertical temperature differences of up to about 0.01°C instead of <0.0002°C under NH (Fig. 1c). This variability is attributed to (sub-)mesoscale eddy activity related with variations in continental-boundary flow by atmospheric forcing. The switch between the two deep-sea conditions occurs about every 20-30 days and is found year-around, with some increase in activity during winter.

Over a relatively long 11-day NH-episode, semidiurnal variations in pressure, which reflect surface barotropic tidal elevations, match in size near-bottom temperature variations after considering (2), see

https://doi.org/10.5194/egusphere-2026-188
Preprint. Discussion started: 29 January 2026

Fig. 2. We focus on temperature from T-sensors closest to the seafloor, because of all T-sensors these are least collecting (sub-)mesoscale, baroclinic internal wave and turbulence motions. Lesser diurnal and fourth-diurnal peaks in pressure do not stand out from the broad variance in temperature. In contrast, waterflow variations show less semidiurnal variation with time, and instead have dominant response around f, and at sub-mesoscales. At the inertial frequency, pressure variations are very weak and temperature variations are part of a broadband continuum.

The 44-line averaged temperature spectra show a considerable smoothing over the 1-line spectrum at most frequencies, except at the semidiurnal tidal frequency (Fig. 2b, c). This exception suggests a deterministic signal rather than a quasi-randomly distributed spectral content. Band-pass filtered temperature matches (Γ-transferred) pressure semidiurnal lunar M_2 peaks thus well (Fig. 2a), especially in the mid-half of the time series, that the barotropic surface tide explains about 75% of its variance in this narrow frequency band. The barotropic tide can be relatively easily removed, from this record: The pressure-data filtered spectrum in Fig. 2 lacks a peak around M_2.

However, in time-depth images the removal of the deterministic-narrowband barotropic tide does not very clearly show, except in the center of the record (Fig. 3). This is because the barotropic M_2-motions are embedded in broadband, less deterministic and more stochastic, baroclinic internal tide motions that fill the near-bottom IGW-band almost like flat white noise (Fig. 2b, c). As the example is dominated by turbulent convection from below governed by geothermal heating, apparent near-tidal columns are most intensified near the seafloor (Fig. 3). The removal of the barotropic tide smooths the edges of the convection plumes, which have a dominant frequency varying between f and about $2\Omega \approx \omega_{max}$.

From another 11-day example of NH, the IGW bounds retain most IGW-temperature variance in the otherwise slightly sloping band of baroclinic waves (Fig. 4). Compared with Fig. 2, near-inertial waterflow motions are slightly reduced in this example, or spread over a wider band of (super-inertial) frequencies. As in the previous example, barotropic signals take up a considerable part, explaining about 50% of variance of the semidiurnal near-bottom temperature signals. Their removal via the pressure record and (2) has slightly more visual effect (Fig. 5), not only in the center of the time series, but also

https://doi.org/10.5194/egusphere-2026-188
Preprint. Discussion started: 29 January 2026

near the beginning. In contrast with Fig. 2, the entire IGW- and sub-inertial bands show less smoothing for the 44-line average spectrum (Fig. 4b, c). This suggests more coherent motions at these frequencies than in the example of geothermally dominated turbulence convection, possibly associated with the somewhat larger temperature variance in the IGW band of Fig. 4.

The removal of barotropic signals via pressure record is unnecessary under SW conditions, when temperature variations in the IGW band and at sub-mesoscales are larger by one order of magnitude, two orders in variance, see the 11-day example in Fig. 6. The IGW-band is almost flat in variance distribution (Fig. 6b, c), as in Fig. 2. The 44-line average spectrum is only smoothed for $\omega > 10$ cpd, which demonstrates a considerable extent in frequency range of coherent motions, in comparison with Figs 2 and 4. With the increased overall IGW-variance in temperature, which correlates in-phase with acoustic reflection (van Haren et al., 2026), the waterflow spectrum shows a smaller inertial peak than in Fig. 4 besides increased sub-mesoscale/sub-inertial-IGW activity.

Semidiurnal pressure and temperature signals not only differ strongly in amplitude, but also in phase (Fig. 6a). As a result, temperature is dominated by baroclinic internal wave signals, which, however, still show a small semidiurnal peak (Fig. 6b,c). Essentially, this small peak is not at M_2, but around $2\Omega \approx \omega_{max}$ (for $N < 0.5f$). The small temperature peak near the upper IGW-bound is surprising considering that mean $N \approx 2.2f \approx 3$ cpd (cycles per day), a clear shift to higher frequencies in comparison with the NH examples in Figs 2 and 4. However, the relative peak at about 0.27 cpd may be equivalent to ω_{min} for $N = 0.3f$ (for which $\omega_{max} = 2.03$ cpd). This difficult-to-measure small N suggests that the apparently stable SW conditions are actually very weakly stratified, in their direction of turbulent convection that is slanted away from gravity.

Slantwise convection leads to a widening of the IGW range, apparently with some enhancements near its bounds including baroclinic semidiurnal internal wave motions, like observed in the present deep Mediterranean data. As the convection is governed by highly nonlinear processes, the associated relatively strong turbulence that is elevated by one order of magnitude over open-ocean values seems to be important for the replenishment of nutrients in the deep Mediterranean. This is subject of future study.

https://doi.org/10.5194/egusphere-2026-188
Preprint. Discussion started: 29 January 2026

4 Discussion and Conclusions

Future studies using yearlong data in the deep Northwestern Mediterranean need not much concern about barotropic surface tidal signals spoiling baroclinic internal wave signals. The barotropic tides are weak, and only show O(0.00001°C) in temperature records under near-homogenous conditions. Such small temperature signals are successfully corrected using pressure information and local adiabatic lapse rate. The use of Γ is further investigated for correction of precise positioning of different mooring lines attached to the doming cable grid (van Haren, 2026, submitted).

Indirectly though barotropic tides potentially may have effect after sufficient energy transfer to baroclinic IGW. In the present data such a transfer is not well observed, as under NH semidiurnal temperature variations are mainly attributable to barotropic sealevel variations. Under SW, no dominant lunar semidiurnal signals are observed, and semidiurnal variations are associated with the maximum IGW bound. Likewise, no semidiurnal lunar peak is observed in waterflow spectra.

Under NH, the observed broadband spread of temperature variance throughout IGW is attributable to N < f, confirming non-traditional internal wave frequency bounds. Small peaks occur at the bounds and reflect some wave trapping. The lower IGW-bound extends well into the sub-mesoscale range. No effect of eddies is observed, although waterflow demonstrates a small peak around 1.2f.

Under SW, the elevated temperature variance shows basically the same IGW-spread as under NH, which does not comply with local mean N. Instead, it reflects an IGW for very weak N ≈ 0.3f. Or, it reflects a band-widening indeed by local relative vorticity as the waterflow spectrum suggests peaks at 0.5f, f, 1.5f, in decreasing order. This requires further investigation on the interaction between sub-mesoscale and IGW motions.

Data availability. Only raw data are stored from the T-sensor mooring-array. Analyses proceed via extensive post-processing, including manual checks, which are adapted to the specific analysis task. Because of the complex processing the raw data from the custom-made T-sensors are not made publicly accessible. Current meter and CTD data are available from van Haren (2025): “Large-ring mooring current meter and CTD data”, Mendeley Data, V1, https://doi.org/10.17632/f8kfwcvtdn.1.

https://doi.org/10.5194/egusphere-2026-188
Preprint. Discussion started: 29 January 2026

Competing interests. The author has no competing interests.

Acknowledgments. This research was supported in part by NWO, the Netherlands organization for the advancement of science. Captains and crews of R/V Pelagia are thanked for the very pleasant cooperation. NIOZ colleagues notably from the NMF department are especially thanked for their indispensable contributions during the long but very pleasant preparatory and construction phases of the large-ring mooring to make this unique sea-operation successful. I am indebted to colleagues in the KM3NeT Collaboration, who demonstrated the feasibility of deployment of large three-dimensional deep-sea research infrastructures. V. Bertin helped with local organization in La Seyne-sur-mer.

https://doi.org/10.5194/egusphere-2026-188
Preprint. Discussion started: 29 January 2026

References

Crepon, M., Wald, L., and Monget, J. M.: Low frequency waves in the Ligurian Sea during December 1977, J. Geophys. Res., 87, 595-600, 1982.

Ferron, B., Bouruet Aubertot, P., Cuypers, Y., Schroeder, K., and Borghini, M.: How important are diapycnal mixing and geothermal heating for the deep circulation of the Western Mediterranean? Geophys. Res. Lett., 44, 7845-7854, 2017.

Garrett, C.: The Mediterranean Sea as a climate test basin, In: Malanotte-Rizzoli, P., and Robinson, A. R. eds., Ocean Processes in Climate Dynamics: Global and Mediterranean Examples, Kluwer Academic Publishers, 227-237, 1994.

Gerkema, T., Zimmerman, J. T. F., Maas, L. R. M., and van Haren, H.: Geophysical and astrophysical fluid dynamics beyond the traditional approximation, Rev. Geophys., 46, RG2004, doi:10.1029/2006RG000220, 2008.

IOC, SCOR, and IAPSO: The International Thermodynamic Equation of Seawater – 2010: Calculation and Use of Thermodynamic Properties, Intergovernmental Oceanographic Commission, Manuals and Guides No. 56, UNESCO, Paris, 196 pp, 2010.

Kunze, E.: Near-inertial wave propagation in geostrophic shear, J. Phys. Oceanogr., 15, 544-565, 1985.

LeBlond, P. H., and Mysak, L. A.: Waves in the Ocean, Elsevier, New York, 602 pp, 1978.

Marshall, J., and Schott, F.: Open-ocean convection: Observations, theory, and models, Rev. Geophys., 37, 1-64, 1999.

Sheremet, V. A.: Laboratory experiments with tilted convective plumes on a centrifuge: A finite angle between the buoyancy force and the axis of rotation, J. Fluid Mech., 506, 217-244, 2004.

Straneo, F., Kawase, M., and Riser, S. C.: Idealized models of slantwise convection in a baroclinic flow, J. Phys. Oceanogr., 32, 558-572, 2002.

Testor, P., and Gascard, J.C.: Post-convection spreading phase in the Northwestern Mediterranean Sea, Deep-Sea Res., 53, 869-893, 2006.

van Haren, H.: Philosophy and application of high-resolution temperature sensors for stratified waters, Sensors, 18, 3184, doi:10.3390/s18103184, 2018.

https://doi.org/10.5194/egusphere-2026-188
Preprint. Discussion started: 29 January 2026

van Haren, H.: Thermistor string corrections in data from very weakly stratified deep-ocean waters, Deep-Sea Res. I, 189, 103870, 2022.

van Haren, H., and Millot, C.: Seasonality of internal gravity waves kinetic energy spectra in the Ligurian Basin, Oceanol. Acta, 26, 635-644, 2003.

van Haren, H. et al.: High-frequency internal wave motions at the ANTARES site in the deep Western Mediterranean, Ocean Dyn., 64, 507-517, 2014.

van Haren, H., Bakker, R., Witte, Y., Laan, M., and van Heerwaarden, J.: Half a cubic hectometer mooring-array 3D-T of 3000 temperature sensors in the deep sea, J. Atmos. Ocean. Technol., 38, 1585-1597, 2021.

van Haren, H., et al.: Whipped and mixed warm clouds in the deep sea, Geophys. Res. Lett., in press, 2026.

Wunsch, C., and Ferrari, R.: Vertical mixing, energy, and the general circulation of the oceans, Annu. Rev. Fluid Mech., 36, 281-314, 2004.

https://doi.org/10.5194/egusphere-2026-188
Preprint. Discussion started: 29 January 2026

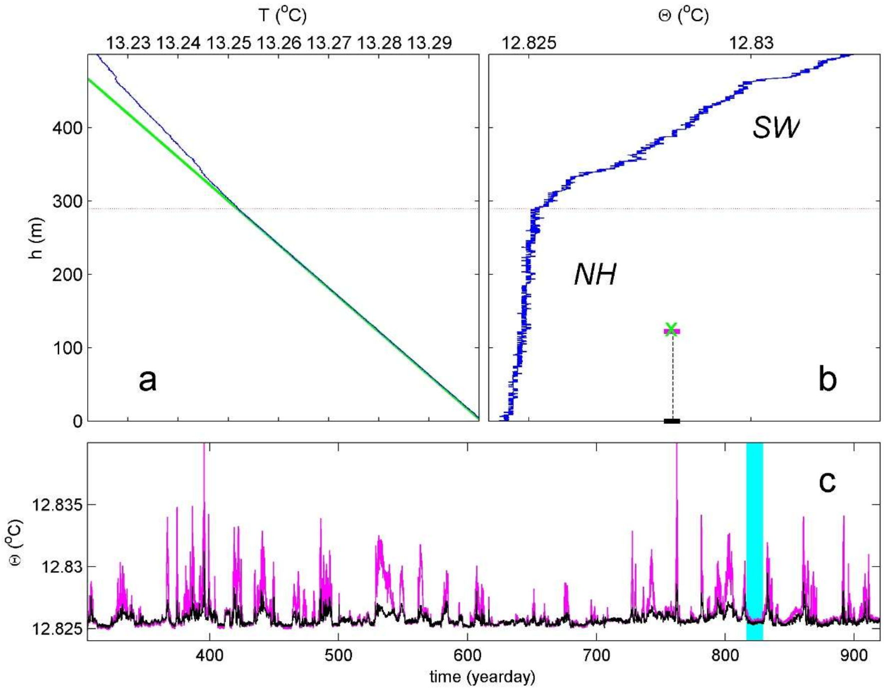

Figure 1. Data overview from deep Mediterranean at the site of the large-ring mooring. (a) Uncorrected temperature from lower 500 m of shipborne CTD profile. In green, the local adiabatic lapse rate starting at the temperature observed at h = 0.5 m above seafloor. (b) Pressure-corrected Conservative Temperature (IOC et al., 2010) together with locations of uppermost (magenta) and lowest (black) moored temperature 'T'-sensors, and (green x) moored current meter 'CM'. SW = stratified water, NH = near-homogenous. (c) Entire 600-d time series of uppermost and lowest moored T-sensor data from one line, with episode in Figs 2, 3 highlighted. Time is given in days of 2020 (+365 in 2021).

https://doi.org/10.5194/egusphere-2026-188
Preprint. Discussion started: 29 January 2026

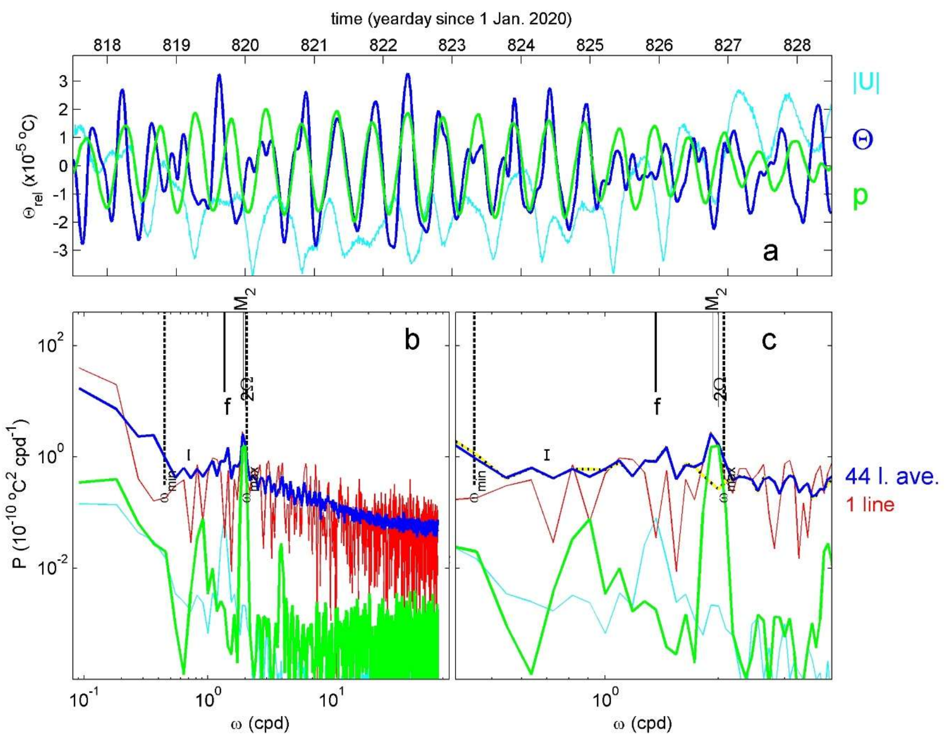

Figure 2. Magnification of 11 days of data under near-homogeneous 'NH' conditions from near-bottom h≈2-m T-sensors and upper-range h=126-m CM's, all (sub-)sampled at once per 600 s. (a) Time series comparison between records relative to their mean value of semidiurnal band-pass filtered 'bpf' temperature (blue; average over 44 lines), bpf pressure (green; transferred to temperature via the local adiabatic lapse rate; average over 3 CM's), and low-pass filtered waterflow amplitude (cyan; arbitrary units; average over 3 CM's). (b) Energy spectra for records in a., together with temperature from one line (red). The error bar is for 44-line smoothed data. Besides inertial frequency f, semidiurnal 2Ω, and lunar M_2, inertio-gravity wave 'IGW' bounds [ω_{min} ω_{max}] are indicated for buoyancy frequency N = 0.5f. (c) One-decade zoom on IGW from b., with the addition of pressure-data filtered 44-line mean temperature spectrum (dashed black-yellow).

https://doi.org/10.5194/egusphere-2026-188
Preprint. Discussion started: 29 January 2026

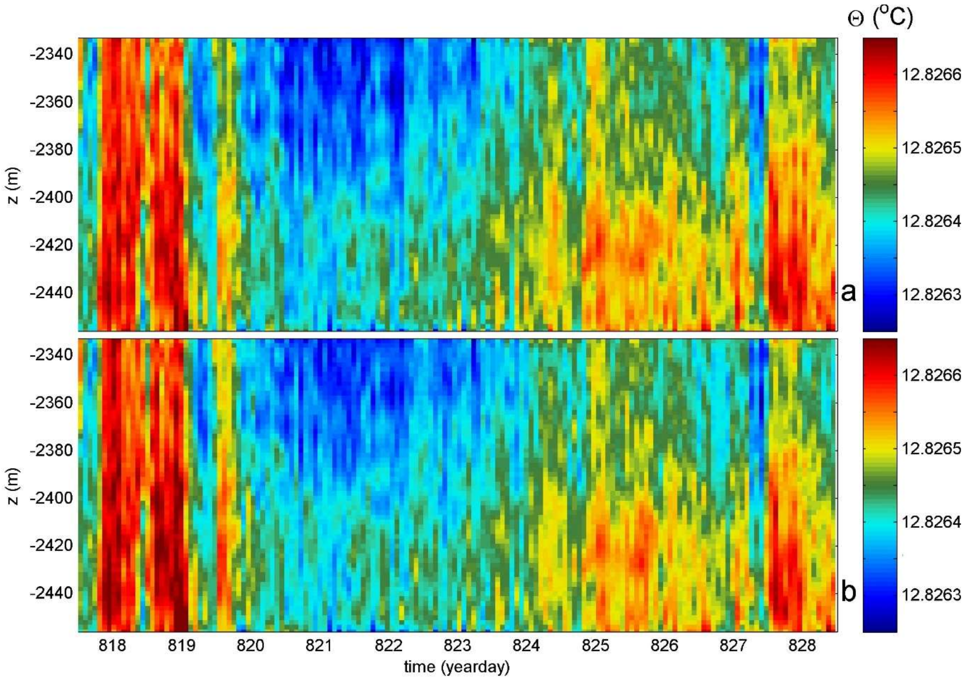

Figure 3. Effect of pressure-data filtering on 600-s sub-sampled temperature data from one line for NH in Fig. 2 that is dominated by geothermal heating. (a) Time-depth plot of Conservative Temperature after common post-processing (van Haren, 2018). (b) Data from a., after additional barotropic-tidal filtering using pressure data.

https://doi.org/10.5194/egusphere-2026-188
Preprint. Discussion started: 29 January 2026

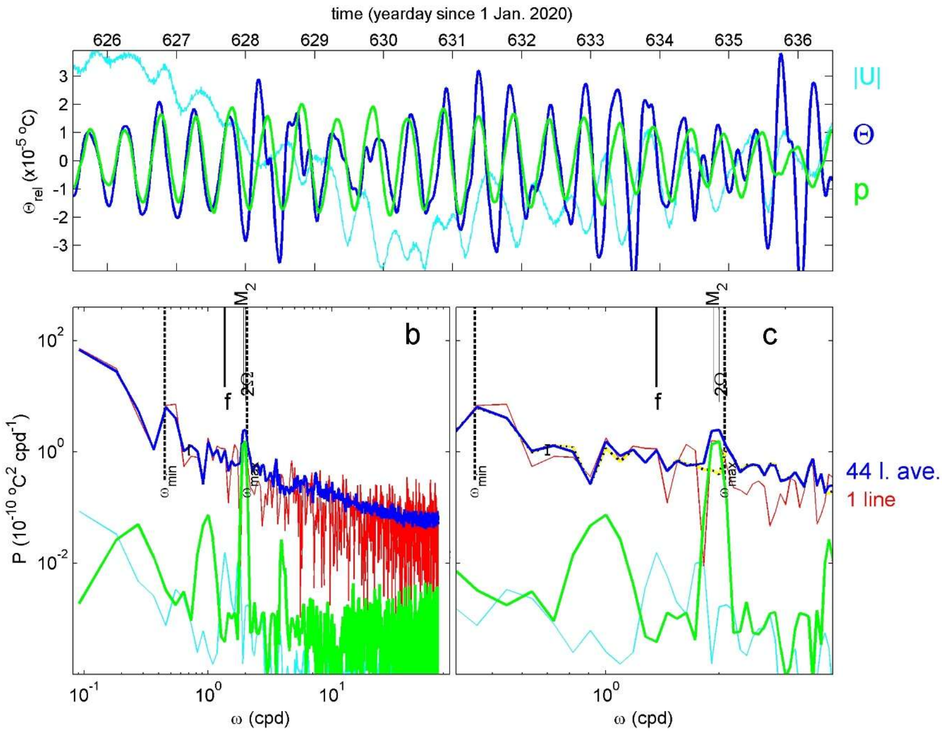

Figure 4. As Fig. 2, but for different NH-conditions.

https://doi.org/10.5194/egusphere-2026-188
Preprint. Discussion started: 29 January 2026

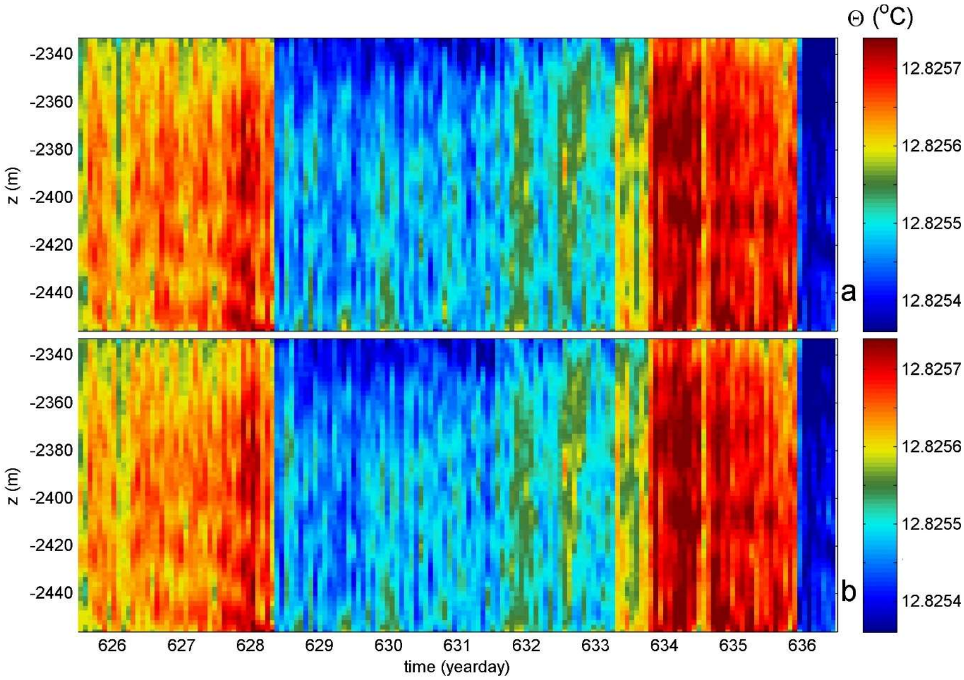

297

298 **Figure 5.** As Fig. 3, but for NH of Fig. 4, which is dominated by >125-m tall vertical "columns".

299

https://doi.org/10.5194/egusphere-2026-188
Preprint. Discussion started: 29 January 2026

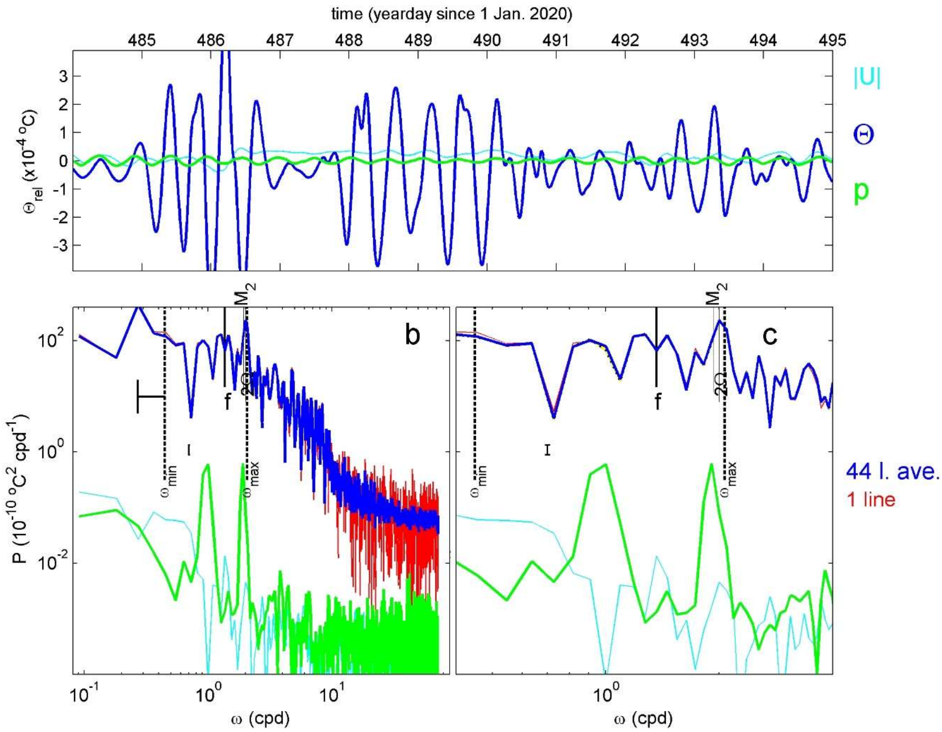

Figure 6. As Fig. 2, but for stratified water conditions. The 90°-rotated-T extension to the ω_{min}-bound in b. is for N = 0.3f (see text). The y-axis range in a. is 10 times larger than in Fig. 2a.